Accepted Manuscript

Formation and characteristic corrosion behavior of alternately lamellar arranged α and β in as-cast AZ91 Mg alloy

Ying-Chao Zhao, Ming-Chun Zhao, Rong Xu, Long Liu, Jun-Xi Tao, Chengde Gao, Cijun Shuai, Andrej Atrens

PII: S0925-8388(18)32976-1

DOI: 10.1016/j.jallcom.2018.08.103

Reference: JALCOM 47191

To appear in: *Journal of Alloys and Compounds*

Received Date: 13 April 2018

Revised Date: 26 July 2018

Accepted Date: 11 August 2018

Please cite this article as: Y.-C. Zhao, M.-C. Zhao, R. Xu, L. Liu, J.-X. Tao, C. Gao, C. Shuai, A. Atrens, Formation and characteristic corrosion behavior of alternately lamellar arranged α and β in as-cast AZ91 Mg alloy, *Journal of Alloys and Compounds* (2018), doi: 10.1016/j.jallcom.2018.08.103.

Formation and characteristic corrosion behavior of alternately lamellar arranged α and β in as-cast AZ91 Mg alloy

Ying-Chao Zhao [a,b], Ming-Chun Zhao[b,*], Rong Xu[b], Long Liu[c], Jun-Xi Tao[b], Chengde Gao [c], Cijun Shuai [c], Andrej Atrens [d,*]

[a], Light Alloy Research Institute, Central South University, Changsha 410083, P.R. China

[b], School of Materials Science and Engineering, Central South University, Changsha 410083, P.R. China

[c],College of Mechanical and Electrical Engineering, Central South University, Changsha 410083, P.R. China

[d], Division of Materials, The University of Queensland, Brisbane, Qld 4072, Australia

*Corresponding authors: Prof. Ming-Chun Zhao, Email: mczhao@csu.edu.cn;

Prof. Andrej Atrens, Email: andrejs.atrens@uq.edu.au;

Abstract: Formation and characteristic corrosion resistance of alternately lamellar arranged α and β in as-cast AZ91 Mg alloy were investigated as an independent micro-constituent identity. As-cast AZ91 presented three microstructural entities, i.e. α-Mg grain, (α+β) lamellae and coarse β particle, and each had its own Al content and microstructural morphology. The lamellae occurrence was due to the precipitation of β particle from the divorced eutectic Al-rich-α phase during solidification, because the Al composition can not exceed its maximum solubility. The evidences that were obtained from electrochemical tests, micro-corrosion morphology and hydrogen evolution rate certified that the (α+β) lamellae was beneficial to corrosion resistance, which was different from the reported deleterious influence for its original eutectic Al-rich-α phase. This different corrosion behavior was explained to be ascribed to the changes in fine structure and local composition that resulted in combined electrochemical effects of the changes in α and β phases on the corrosion.

Keywords: AZ91 Mg alloy; micro-constituent identity; formation; corrosion; eutectic phase.

1. Introduction

Mg alloys have a high strength-to-weight ratio, and have significant potential in the automotive, aerospace and electronic industries where weight reduction is a necessary requirement. AZ91 is one of the most popular Mg alloys for current commercial applications, offering a good combination of castability, corrosion resistance and mechanical properties compared to other Mg alloys [1-4]. The microstructure of AZ91 typically contains a matrix of α-Mg grains and the second β phase particles (consisting of the intermetallic $Mg_{17}Al_{12}$) distributed along the α-Mg grain boundaries [5-12]. The typical β particle in the microstructure of die-cast AZ91 is typically surrounded by an Al-rich-α area [7-12], and the final microstructure consists of an α-Mg matrix, coarse β particles and Al-rich-α areas. Song et al [7] considered that the Al-rich-α area and β particles in die-cast AZ91 are derived from an eutectic reaction, so that the phases can be designated as eutectic Al-rich-α Mg and eutectic β. Alternatively, a lamellae containing α and the fine β particles, i.e. (α+β) lamellae, may occur for AZ91 for some casting solidification conditions, i.e. the microstructure of as-cast AZ91 consisted of (α+β) lamellae surrounding the coarse β particles rather than Al-rich-α areas surrounding the coarse β particles [6-7, 13-14]. Formation of (α+β) lamellae in as-cast AZ91 is an interesting phenomenon. An explanation was given for the formation of the (α+β) lamellae to be similar to the typical lamellar pearlite colony in steels [13-14]. The nucleation and growth of pearlite in steels involves in phase change in an eutectoid reaction: the face centered cubic austenite phase (γ) transforms into (i) the body centered cubic ferrite phase (α_F) and (ii) the complex oblique structure cementite phase (Fe_3C). These three phases have different crystal structures. However, it is worth noting that the α phase and the β phase in lamellae of as-cast AZ91 do not derive from a different new phase but derive from a Al-rich α phase that has the same crystal structure as the α phase, although the morphology with an alternately lamellar arranged fine α plate and fine β plate is highly similar to pearlite. The detailed forming processes of (α+β) lamellae in as-cast AZ91 needs further investigation.

For commercial utilization of AZ91, a significant limitations for potential use is its corrosion behavior, which can be significantly influenced by the distribution and morphology of the second phase particles in the matrix of α-Mg grains [15]. The prior researches [6-7] demonstrated that the second β phase particles in AZ91 served two roles: (i) as

a barrier to stop the corrosion progression when the β phase is continuous and the fraction is high, and (ii) as a galvanic cathode to accelerate the corrosion when the β phase fraction is low and finely divided. However, much effort concerning the role of second phase on the corrosion behaviors of AZ91 has focused on the microstructures consisting of the coarse β-phase particles surrounded by Al-rich-α area rather than the microstructures consisting of the coarse β phase particles surrounded by the alternately lamellar arranged α and β phases [5-9]. Zhao et al [13-14] demonstrated that in AZ91, the as-cast condition with the fine (α+β) lamellae had lower corrosion rates than AZ91 in heat-treated conditions which completely eliminated the (α+β) lamellae. Accordingly, the fine (α+β) lamellae was inferred to decrease the corrosion rate, which was different from a reported deleterious influence to corrosion resistance of the original Al-rich-α area in die-cast AZ91 [7, 9]. In these cases, however, the researches mainly focused on the influence of heat treatment on microstructure evolution and corrosion. An understanding of the electrochemistry of the fine (α+β) lamellae has not yet been clarified, and the mechanism by which the fine (α+β) lamellae influences corrosion behavior is not known; nor is the difference of corrosion behavior of the fine (α+β) lamellae and the original Al-rich-α area. What is needed is an understanding of the corrosion behavior of the alternately lamellar arranged α and β and of the Al-rich-α area in as-cast AZ91.

This work attempts to clarify these aspects using AZ91 in the as-cast condition containing alternately lamellar arranged α and β in the microstructure, paying special attention to (i) the Al content for the different phases, (ii) the formation processes, (iii) the corrosion susceptibility and (iv) the electrochemical corrosion behavior. The prior research [13-14] showed that the solid-solution heat treatment can progressively dissolve or fully dissolve the β phase in AZ91, and produce a microstructure in which the (α+β) lamellae was eliminated accompanied by (a) without significantly altering the coarse β particles or (b) with completely dissolving the coarse β particles. Therefore, we also investigated solid solution heat treatment conditions which completely eliminated (α+β) lamellae in the microstructure. It is hoped that this investigation will lead to a better understanding of the factors that influence microstructure formation and corrosion behavior of as-cast AZ91 and facilitate its use in practical applications.

2. Experimental procedure

The experimental AZ91 ingot has the following chemical compositions (in wt.%) 8.26 Al, 0.69 Zn, 0.14 Mn, 0.002 Ni, balance Mg. The AZ91 was prepared using pure Mg, Al and Zn. The Mg was melted in an aluminium oxide crucible heated to 720°C. Al and Zn buttons were added to the melt after Mg was completely molten. The melt was stirred until all the buttons dissolved. The crucible was then air cooled to room temperature. All the above procedures were conducted in a flowing protective gas (dry air with 0.25 mol% SF_6) to prevent burning and oxidation. The specimens cut from the as-cast ingot were subjected to the following additional solid solution heat treatment: (i) annealing at 380 ℃ for 25 hours followed by water quenching (hereafter, 3-S), and (ii) annealing at 410℃ for 100 hours followed by water quenching (hereafter, 4-S). Microstructures were examined by optical microscopy and scanning electron microscopy (SEM) after mechanical grinding, polishing, and etching in 3% nital solution. Energy dispersive X-ray spectroscopy (EDS) in a SEM was used to characterize the composition distribution.

Immersion test was conducted at room temperature. Coupons were encapsulated into epoxy resin so that only one working surface was exposed to the 1 M NaCl solution. This immersion test (using only one working surface rather than generally completely immersing the sample in the corrosion solution) provided a metallographic prepared working surface and also decreased any boundary effect. Each working surface was finally ground to 1200 grit SiC paper, washed with distilled water and dried using warm flowing air. The sample was horizontally immersed in the test solution of 1500 ml, the evolved hydrogen was collected into a burette above the corroding sample with the working surface of 18 mm x 27 mm, and the corrosion micro-morphology was examined using optical microscopy. The cathodic reaction is: $2H_2O + 2e \rightarrow H_2\uparrow + 2OH^-$ and the anodic reaction is: $Mg - 2e \rightarrow Mg^{2+}$. The corrosion morphology was also observed for a second series of metallographic prepared specimens, which were removed from the 1 M NaCl solution after various immersion times. After removal from the test solution, the specimens were rinsed with distilled water, dried with flowing air and observed with optical microscopy.

Potentiodynamic polarization curves were measured in 1 M NaCl solution, in a glass cell using a PAR-2263 potentiostat system at a scanning rate of 0.2 mV/s from a cathodic potential to an anodic potential, (i) immediately

after immersion and (ii) 40 h after immersion. Samples for potentiodynamic polarization curves were encapsulated into epoxy resin so that a surface with the dimension of 10 mm x 10 mm was exposed to the 1 M NaCl solution of 500 mL. The sample surface was prepared by mechanical grinding successively to 1200 grit SiC paper and by washing with distilled water. A platinum gauze (25 mm x 25 mm, 52 mesh) was used as a counter electrode, and a saturated calomel electrode (SCE) was used as the reference electrode. All potentials were referred to the SCE.

3. Results

Fig. 1a presents a low magnification view of the microstructure of as-cast AZ91 in an optical micrograph. The microstructure consisted of the α-Mg matrix, the coarse β particles, and some dark hard-to-resolve regions next to the coarse β particles. These dark regions contained alternately arranged α-Mg and the fine β in a lamellae structure as presented at higher magnification in the SEM micrograph in Fig. 1b. The morphology of the fine β particles in the (α+β) lamellae was in the form of long laths and apparently discontinuous short laths. The (α+β) lamellae towards the periphery of the coarse β particle are clearly evident.

Fig. 2 presents the EDS spectra showing the varying composition distribution in the different micro-constituents of the as-cast AZ91 microstructure. An EDS analysis along the line illustrated in Fig. 2a shows that there was a slope of the measured composition of the (α+β) lamellae adjacent to the coarse β particle and essentially constant composition of the α-Mg matrix. Interpretation of the data needs to take into account that the measurement volume is of the order of 10 microns. Thus this data indicated that the Mg content decreased and the Al content increased when micro-constituent changed (i) from the α-Mg matrix to the (α+β) lamellae, and (ii) from the (α+β) lamellae to the coarse β particle. The composition of three different typical micro-constituents was evaluated by the EDS spectra as illustrated in Fig. 2b~2e, in which point 1, point 2, point 3 and point 4 represent the position in the interior of an α-Mg grain, in the vicinity of the (α+β) lamellae, in the (α+β) lamellae, and in the interior of the coarse β particle, respectively. These measurements could not give an indication of the composition distribution within the α-Mg matrix, because the composition measurement of point 2 had a significant contribution from the lamellar micro-constituent. As a result, the Al concentration in the interior of an α-Mg grain appeared to be a little lower than that in the vicinity of the (α+β) lamellae (point 1 with 5.5 wt.% Al, and point 2 with 7.7 wt.% Al). The fine (α+β) lamellae and the

coarse β particle were rich in Al concentration compared to the α-Mg matrix (point 3 with 12.5 wt.% Al, and point 4 with 37.2 wt.% Al).

Fig. 3 presents the SEM microstructures of the 3-S and 4-S conditions. In the 3-S specimen, the fine (α+β) lamellae had completely dissolved with little alteration of the coarse β particles, and the microstructure consisted of the α-Mg matrix plus the isolated coarse β particles. In the 4-S specimen, both the (α+β) lamellae and coarse β particles had completely dissolved into the α-Mg matrix and the microstructure was homogenous α-Mg.

Fig. 4 presents EDS spectra showing the compositions in the micro-constituents of the 3-S condition. Point 1, point 2 and point 3 represent the position in the interior of an α-Mg grain, in the vicinity of the coarse β particle and in the interior of the coarse β particle, respectively. EDS analysis confirmed the presence of the different Al contents in the different micro-constituents (α-Mg matrix, point 1 with 8.5 wt.% Al; in the vicinity of the coarse β particle, point 2 with 9.2 wt.% Al; in the coarse β particle, point 3 with 37.1 wt.% Al). Furthermore, an EDS analysis along the line indicated in Fig. 4 showed the evident composition differences in these phases.

Fig. 5 presents hydrogen evolution volume data. There was an incubation period during which there was a small rate of hydrogen evolution, after which there was an increase in hydrogen evolution volume with increasing immersion time. The quantity of hydrogen evolved was different. At the end of the 96 h immersion period, the as-cast condition had the smallest hydrogen evolution volume, the 4-S condition had more, and the 3-S condition had the most. The hydrogen evolution volume of the as-cast condition was slightly higher than that of the 4-S condition at the beginning 60 h immersion test, but subsequently became lower.

Fig. 6 presents the measured open circuit potential. The potential first increased for several minutes to a maximum consistent with an incubation period for corrosion initiation. The incubation period from the open circuit potential was shorter than that from the hydrogen gas evolution indicating that the electrochemical technique was more sensitive in detecting the onset of localized corrosion than the technique based on hydrogen gas evolution. Subsequently the open circuit potential decreased to more negative values correlating with the increase of corrosion area and the occurrence of corrosion. At the beginning of the onset of local corrosion, the 4-S condition had the most positive open circuit potential, the as-cast condition was in a second position, and the 3-S condition was the most

negative. After arriving at a stable value, the as-cast condition had the most positive open circuit potential, the 4-S condition was in a second position and the 3-S condition was the most negative. There appears to be a good correlation between the open circuit potential and the amount of corrosion as determined from hydrogen evolution that are given in Fig. 5: (i) the 3-S condition has most negative open circuit potential and gives the largest hydrogen evolution volume, and (ii) compared to the 4-S condition, the as-cast condition has more negative open circuit potential at the beginning of the onset of local corrosion and presents higher hydrogen evolution volume in the beginning 60 h immersion test, while has more positive open circuit potential at a stable value correlating with corrosion for some considerable time after onset and presents lower hydrogen evolution volume with further advance of the corrosion attack in immersion test longer than 60 h. The open circuit potential correlation with the level of corrosion as determined from immersion test has been described previously [16] and the present work was consistent in this aspect.

Fig. 7 presents the polarization curves measured after immediate immersion (Fig. 7a) and after 40 h immersion (Fig. 7b). All the polarization curves are similar. The corrosion current density (i_{corr}) for immediate immersion (Fig. 7a), measured from the cathodic branch of the polarization curves, increased in the following order: 4-S condition < as-cast condition < 3-S condition, while the i_{corr} for 40 h immersion (Fig. 7b) increases in the following order: as-cast condition < 4-S condition < 3-S condition. Therefore, the i_{corr} estimated by Tafel extrapolation using polarization curve was consistent with the tendency of the hydrogen evolution volume: (i) the 3-S condition, which has the highest i_{corr} for the immediate immersion and the 40 h immersion, presents the highest hydrogen evolution volume, (ii) compared to the 4-S condition, the as-cast condition had higher i_{corr} for the immediate immersion and presents higher hydrogen evolution volume in the beginning 60 h immersion test, while has lower i_{corr} for the 40 h immersion and presents lower hydrogen evolution volume with further advance of the corrosion attack in immersion test longer than 60 h.

Fig. 8 presents the SEM examination of the corroded surface using carbon-coated specimen after the immersion test. Most of the surface had no corrosion attack, whereas there were some areas as indicated that had relatively deep corrosion. This indicates that the evaluation of the corrosion morphology for these Mg alloys is somewhat difficult

after a long exposure time, as the corrosion region is covered with corrosion products. The un-attacked surface of the specimen was covered by net-like corrosion production layer. The net-like corrosion production is similar in appearance to honeycomb or sponge. The crystals of the corrosion product film grew perpendicular to the substrate metal.

Fig. 9 shows the micro-corrosion morphology of another series of metallographic prepared specimens, which were removed from the 1 M NaCl solution after various immersion times to examine corrosion micro-morphology using optical microscopy. The preferential corrosion attack initiated in the α-Mg matrix region adjacent to the nude coarse β particles in as-cast condition immersed for 1 h (Fig. 9a). Corrosion of the α-Mg was up to the fine (α+β) lamellae with the appearance that the corrosion of the α-Mg stopped at the interface with the fine (α+β) lamellae in as-cast condition immersed for 18 h (Fig. 9b). The α-Mg matrix was corroded leaving the β plates in the lamellar region in as-cast condition immersed for 36 h (Fig. 9c). The isolated coarse β particles in the microstructure did not cause an effective block for the corrosion attack because of large distance between each other in the 3-S condition (Fig. 9d).

Based on the above results, the 4-S condition and the as-cast condition have better corrosion resistance than the 3-S condition, which may be explained to be due to galvanic corrosion between coarse β particles and α-Mg matrix in the 3-S condition, and furthermore, the 4-S condition has better corrosion resistance than the as-cast condition at the beginning corrosion but subsequently becomes worse, which indicated that the advance of corrosion in the as-cast condition is hindered by the (α+β) lamellae.

4. Discussion

4.1 Formation of alternately lamellar arranged α and β

The microstructure (Fig. 1) and the EDX analyses (Fig. 2) indicated there were three microstructural entities in the as-cast AZ91: (i) α-Mg matrix, (ii) (α+β) lamellae and (iii) coarse β particle. These have different overall compositions.

The Mg-Al binary equilibrium phase diagram [17], as shown in Fig. 10, indicates the solid solubility of Al in the

Mg matrix at various temperatures and provides clues to the formation mechanism of each microstructural entity. The maximum solid solubility of Al in α-Mg is about 12.7 wt% at the eutectic temperature of 437℃, and its minimum solid solubility is about 2 wt% at room temperature. However, the actual cooling rate is generally higher than that which allows for equilibrium solidification. As a consequence, the eutectic temperature and the critical hypoeutectic Al content become lower under actual condition than those in equilibrium. The actual solidification is schematically described by the dashed line in the non-equilibrium phase diagram as also shown in Fig. 10. The eutectic solidification reaction occurs to produce α-Mg with a lower Al concentration (C' compared with C) during non-equilibrium solidification of AZ91. During cooling, the liquid first solidifies into proeutectoid or primary α-Mg grains, which were identified in Fig. 1 as the α-Mg matrix. The remaining liquid becomes rich in Al content with a concentration close to the eutectic composition at the end of solidification. Final solidification occurs by a eutectic reaction to transform the final liquid at the eutectic temperature into eutectic α-Mg grains and eutectic β particles. The Al content in AZ91 is far from the eutectic composition, which causes the amount of primary α-Mg to be much higher than that of the eutectic microconstituent. Therefore the eutectic α-Mg solidifies attached to the primary α-Mg dendrite with the same phase structure, while the eutectic β particles are distributed in the sites of final solidification as identified in Fig. 1 as coarse β particles. As a consequence, there is a divorced eutectic, in which eutectic α surrounds eutectic β.

On the further cooling, the α phase containing the primary α and the eutectic α becomes super-saturated in Al concentration according to phase diagram (Fig. 10), especially in the divorced eutectic α grain with its high Al content. The α phase super-saturated in Al precipitates β particles. The β particles precipitate in the eutectic α and produce the lamellar (α+β) morphology shown in Fig. 1. The formation of this lamellar micro-constituent occurs by a precipitation reaction in the eutectic α-Mg grains super-saturated in Al after solidification finishes. During the precipitation, Al is rejected from the super-saturated α-Mg grain. If the Al diffusion is not fast, Al accumulates and forms a β-plate when the Al content reaches a critical value, and then the β-plate grows because of the Al slow diffusion in the super-saturated α-Mg grain. The two sides in vicinity of the β plate have a lower Al content and still remains α phase due to the formation of the Al-rich-β plate from Al diffusion. As a consequence, there is a resulting alternately lamellar arranged β plate precipitate and α-Mg in as-cast AZ91. The growth process is schematically depicted in Fig. 11. Although the morphology of alternate lamellar arranged fine α plate and fine β plate in as-cast

AZ91 is similar to pearlite in steel, it is a single phase precipitation reaction in as-cast AZ91, in which the new phase (precipitated β phase) with a rich solute concentration (Al) precipitated from the mother phase (α-Mg) and the mother phase still maintained the original crystal structure. In other words, as-cast AZ91 is transformed, and the Al-rich α-Mg grains precipitate the second β phase during the slow cooling while still maintain a substantially α-Mg microstructure, i.e. α─ → α+β. This proposed formation mechanism is consistent with the present as-cast AZ91 rather than the die-cast AZ91. Rapid cooling rates applied to die-cast AZ91 can effectively suppress the precipitation of β particles from the eutectic Al-rich-α, which results in only the divorced eutectic coarse β particles and the divorced eutectic Al-rich-α area. The same chemical compositions as the experimental as-cast AZ91 ingot were used to produce die-cast AZ91 by rapidly injecting the melt into a steel die, whose microstructures are shown in Fig. 12. It can been clearly seen that the coarse β particles are surrounded by the Al-rich-α areas, and there are three typical microstructural entities inferred in the die-cast condition, i.e. α-Mg grain, divorced Al-rich eutectic α-Mg and coarse divorced eutectic β. Therefore, the formation of an alternately lamellar arranged fine α plate and fine β plate in as-cast AZ91 is attributed to the relatively slow cooling rate after solidification, which precipitates from the Al-rich-α areas.

The AZ91 specimen, during heating at 380℃ was in the single α-Mg phase field according to the phase diagram, so that the β precipitates in the fine (α+β) lamellae dissolved into the α-Mg matrix and the α-Mg become a supersaturated solid solution at room temperature when water quenched. When the thermal temperature was elevated to 410℃ for 100h (4-S condition), both the (α+β) lamellae and coarse β particles completely dissolved into the α-Mg matrix and a supersaturated single α-Mg solid solution was obtained at room temperature after water quenching. All these changes in microstructure were consistent with the phase diagram in Fig. 10.

4.2 Characteristic corrosion behavior of alternately lamellar arranged α and β

The corrosion testing suggested that the (α+β) lamellae played an important role on the corrosion of as-cast AZ91. The results presented do, however, correlate well with those reported previously. The electrochemical technique was more sensitive in detecting the onset of localized corrosion than the technique based on hydrogen gas evolution, and there is a result that the incubation period from the open circuit potential was shorter than that from the hydrogen gas evolution. Visual observation after the measurement of the polarization curves revealed in each case that the electrode surface was severely corroded and had become black and uneven. The polarization curves for all

conditions were not symmetrical between their anodic and cathodic branches. There were more rapid increases in potential vs log I in the anodic polarization branches than in the cathodic polarization branches. In the cathodic potential range, some pitting corrosion initiated at some sites on the surface in each case, but the other sites on surface remained bright and did not change during the polarization measurements. However just around the corrosion potential, pitting corrosion expanded on the surface and the localized corrosion areas enlarged with increasing potential and time. Hydrogen bubbles evolved mainly from the localized corrosion areas. The hydrogen evolution became more intensive with increasing localized corrosion areas and with increasing potential and time. This is the negative difference effect [18]. The non-symmetrical polarization curve between their anodic and cathodic branches in each case may be ascribed to the complicated anodic polarization behavior of Mg alloys. The surface film around the corrosion potential or in the anodic range is imperfect. Some areas are broken and the substrate metal is exposed to the solution directly. Two reasons were presented for the complicated nature of the anodic polarization curves [6-7]: (I) the simultaneous combination of both anodic dissolution and cathodic hydrogen evolution in the anodic region, and (II) the occurrence of localized corrosion, which could make the anodic process unstable.

The corrosion from the Tafel extrapolation for the immediate immersion related to the onset of corrosion, whereas the corrosion from the hydrogen evolution measurement in the immersion test and from the Tafel extrapolation at 40 h immersion related to corrosion at some considerable time after corrosion onset, when the corrosion was well established. Therefore, compared to the 4-S condition, the as-cast condition has (i) a higher i_{corr} for the immediate immersion while a lower i_{corr} for the 40 h immersion, and (ii) a higher hydrogen evolution volume in the beginning 60 h immersion test while a lower hydrogen evolution volume with further advance of the corrosion attack in immersion test longer than 60 h. This indicates that the fine ($\alpha+\beta$) lamellae in as-cast AZ91 was beneficial to corrosion resistance with advance of the corrosion attack.

As shown in Fig. 9a, the preferential corrosion initiation occurred, but the corrosion attack was not in fact in the vicinity of ($\alpha+\beta$) lamellae. The occurrence of such corrosion initiation may be ascribed to a sufficiently strong galvanic effect between the nude coarse β particle and its adjacent α-Mg matrix. AZ91 has a multiphase microstructure, in which different micro-constituents may form a micro-cell. Usually, α-Mg matrix acts as the anode owing to its much higher Mg composition while the intermetallic β phase acts as the cathode [6-7]. As indicated by EDS in Fig. 2, the composition distribution was not uniform and the Al concentration varied from a few percent in the

α-Mg matrix to 12.5 wt.% in the (α+β) lamellae and to 37.2 wt.% in the coarse β phase particle. Since the different micro-constituents contain different Al levels, their electrochemical behavior may be different. This means that the micro-galvanic corrosion between different micro-constituents could occur. The sudden change of the composition distribution between the nude coarse β particles and their adjacent α-Mg matrix was the largest in terms of the EDS analysis spectra (Fig. 2). Therefore, here the corrosion attack preferentially initiated. As shown in Fig. 9b, there were the following cases: (i) corrosion of the adjacent α-Mg with no significant corrosion of the fine (α+β) lamellae and the coarse β particles, and (ii) corrosion of the α-Mg up to the fine (α+β) lamellae, with the appearance that the corrosion of the α-Mg stopped at the interface with the fine (α+β) lamellae. As shown in Fig. 9c, the α-Mg matrix was corroded leaving the β plates in the lamellar region. Therefore, as stated above, the (α+β) lamellae themselves were relatively stable in the test solution and were somewhat inert to corrosion attack. In this case, even though some surrounding α-Mg grains were corroded, the others should be under the region of the continuous (α+β) lamellae when the α-Mg matrix in the top layer has been dissolved. On the other hand, during corrosion, the α-Mg grains would dissolved preferentially whereas most of the β particles were left on the surface except for some which had been undermined and had fallen out because their surrounding α-Mg matrix had been preferentially dissolved. Hence the β fraction on the sample surface could not be constant during corrosion. It changed from the initial β surface fraction characteristic of the sample surface to a steady state surface fraction determined by the preferential corrosion of the α grains and the undermining of the β phase particles. The independence of (α+β) lamellae as an electro-chemical entity was involved in the relative contributions or a competitive result of the micro-galvanic corrosion and the corrosion barrier. It is easy to imagine that the corrosion initiated and gradually advanced by the dissolution of the α-Mg matrix. When the propagation of the corrosion attack reached the region of the continuous (α+β) lamellae, the corrosion was retarded in a certain extent. Furthermore, the β fraction increased with the advance of the corrosion. Therefore, compared to the 4-S condition with homogenous single α phase, there were the phenomena: (i) the hydrogen evolution volume of the as-cast condition with continuous (α+β) lamellae was slightly higher in the beginning of the 60 h immersion test, but becomes slower with increasing corrosion attack (Fig. 5), and

(ii) the as-cast condition had higher i_{corr} for the immediate immersion (Fig. 7a) relating to the onset of the corrosion of the freshly prepared work surface, while a lower i_{corr} for the 40 h immersion (Fig. 7b) relating to corrosion for some considerable time after onset of corrosion, when the corrosion was well established. For the 3-S condition, the isolated coarse β particles in the microstructure did not cause an effective block for the corrosion attack because of large distance between each other as shown in Fig. 9d. These coarse β particles were a considerable cathode and directly form a cell with the α-Mg matrix, resulting in a significant micro-galvanic corrosion. This was consistent with the measured corrosion data as shown in Fig. 5, i.e. the 3-S condition has the highest the hydrogen evolution volume. For the 4-S condition, almost all β phase particles were dissolved as shown in Fig. 3b. As a consequence, there was little galvanic corrosion and the corrosion attack mainly involved the dissolution of α-Mg in the aqueous solution.

The original Al-rich-α area that precipitated the (α+β) lamellae was believed to have a deleterious influence to corrosion resistance of die-cast AZ91 [7, 9] while the (α+β) lamellae in as-cast AZ91 was beneficial to corrosion resistance in the present experiment. The predominant factors determining the rate of galvanic corrosion include the anode-to-cathode area ratio and difference in potentials of different phases [19]. The composition distribution in AZ91 was not uniform, and Al concentration varied from a few percent in the α matrix to 12 % in the vicinity of the β particle, i.e. the original Al-rich-α area, as reported in Refs. [8, 20-21], and from a few percent in the α-Mg matrix to 12.5 wt.% in the (α+β) lamellae and to 37.2 wt.% in the coarse β particle in the present experiment, as shown in Fig. 2. It has been believed that the phase with a low Al content exhibited higher anodic activity than that for a phase with a high Al content and hence a higher Al content could lead to a lower corrosion rate in Mg alloys [8-9, 22]. Since the α matrix, Al-rich-α area or (α+β) lamellae, and coarse particle contain different Al levels as demonstrated above, their potential could not be the same and they may form a cell to each other. The composition should be crucial to the corrosion behavior. In AZ91 with the original Al-rich-α area, it was suggested that the eutectic α area, i.e. the original Al-rich-α area, may behavior independently as a pseudo-phase [23]. This was the eutectic alpha-phase and was distinct from the primary alpha. A schematic of the relative sizes of Al-rich α and β for die-cast AZ91 and (α+β) lamellae and β for as-cast AZ91 is given in Fig. 13, which is derived from the microstructural characteristics of Fig. 1 and Fig. 12, respectively. The cathodic coarse β particle directly forms a cell with the anodic original Al-rich-α area in priority by considering the difference of Al concentration, and hence the geometrical conditions (i.e. cathode-to-anode

area ratio) would be far more significant to galvanic corrosion in this case compared to the case that the cathodal coarse β particle directly forms a cell with the anodic matrix. In contrast, when the (α+β) lamellae precipitates from the original Al-rich-α area, the original high Al area is covered by the fine (α+β) lamellae containing α and the equilibrium precipitate β and the amount of Al in solid solution in these areas decreases dramatically (as a result of the precipitation reactions). In the (α+β) lamellae area derived from the original Al-rich-α area, the fine β precipitates form a discontinuous β phase barrier as shown in Fig. 1b, which can stop the corrosion evolution to some extent. Therefore, the replacement of high Al areas in the original Al-rich-α area by β precipitates will lead to a decrease in corrodible surface and an increase in the continuity (i.e. effective length) of the corrosion barrier. On the other hand, the discontinuous (lamellar) α phase (separated by the discontinuous lamellar β precipitates) may have a lower Al concentration and could have less corrosion resistance than the original Al-rich-α area. However, the discontinuous (lamellar) α phase was very close to the discontinuous β precipitates and corrosion could be quickly stopped by the adjacent discontinuous β precipitates.

5. Conclusions

1. As-cast AZ91 in the present work presented three microstructural entities, i.e. α-Mg grain, (α+β) lamellae and coarse β particle, and each had its own Al content and microstructural morphology. The formation of the different micro-constituents might be understood from the Mg-Al binary phase diagram. α-Mg grains and coarse β particles derived from the divorced eutectic reaction, while (α+β) lamellae derived from the precipitation reaction, i.e. (α+β) lamellae precipitated from the original eutectic Al-rich-α area.

2. An independent electrochemical identity of the (α+β) lamellae in the eutectic α-phase was investigated by immersion test and electrochemistry measurements. The (α+β) lamellae was beneficial to corrosion resistance. When the propagation of the corrosion attack reached the region of the continuous (α+β) lamellae, the corrosion was retarded to a certain extent, which was also well consistent with the data determined from the hydrogen evolution volume and electrochemistry measurement.

3. The different corrosion behaviors between the (α+β) lamellae and its original eutectic Al-rich-α area were attributed to the changes in microstructures and local compositions. These changes resulted in a combined

electrochemical effects of the changes in α and β phases on the corrosion.

Acknowledgements

This work was supported by the following funds: (1) The Natural Science Foundation of China (51575537, 81572577); (2) Hunan Provincial Natural Science Foundation of China (14JJ1006, 2016JJ1027).

References:

1. T. Jin, Z.W. Zhou, J. Qiu, Z.H. Wang, D. Zhao, X.F. Shu, S.R. Yan, J. Alloys Compd. 738 (2018) 79-88 .

2. J.U. Lee, S.H. Kim, Y.J. Kim, S.H. Park, Mater. Sci. Eng. A 714 (2018), 49-58.

3. M. Zha, H.M. Zhang, C. Wang, H.Y. Wang, E.B. Zhang, Q.C. Jiang, J. Alloys Compd. 728 (2017),682-693.

4. M.C. Zhao, P. Schmutz, S. Brunner, M. Liu, G.L. Song, A. Atrens, Corro. Sci. 51 (2009) 1277-1292.

5. M.S. Dargusch, M. Nave, S.D. McDonald, D.H. StJohn, J. Alloys Compd. 492 (2010) L64-L68.

6. G.L. Song, A. Atrens, X.L. Wu, B. Zhang, Corr. Sci. 40 (1998) 1769-1791.

7. G.L. Song, A. Atrens, M. Dargusch, Corro. Sci. 41 (1999) 249-273.

8. O. Lunder, J.E. Lein, T.K. Aune, K. Nisancioglu, Corro. 45 (1989) 741-748.

9. R.K. Singh Raman, Metall. Mater. Trans. A 35A (2004) 2525-2531.

10. M.W. Wu, L. Hua, S.M. Xiong, China Foundry 15 (2018) 58-65.

11. L.G. Bland, L.C. Scully, J.R. Scully, Corro. 73 (2017), 526-543.

12. H. Feng, S.H. Liu, Y. Du, T. Lei, R.C. Zeng, T.C. Yuan, J. Alloys Compd. 695 (2017), 2330-2338

13. M.C. Zhao, M. Liu, G.L. Song, A. Atrens, Adv. Eng. Mater. 10 (2008), 93-103.

14. M.C. Zhao, M. Liu, G.L. Song, A. Atrens, Corro. Sci. 50 (2008), 1939-1953.

15. A. Atrens, G.L. Song, M. Liu, Z. Shi, F. Cao, M.S. Dargusch, Adv. Eng. Mater. 17 (2015) 400-453.

16. R.K.S. Raman, N. Birbilis, J. Efthimiadis, Corro. Eng. Sci. Tecnol. 39 (2004) 346-350.

17. A. Monas, O. Shchyglo, S.J. KIM, C. D. Yim, D. Hoche, I. Steinbach, JOM 67 (2015) 1805-1811.

18. G.L. Song, K.A. Unocic, Corr. Sci. 98 (2015) 758-765.

19. M.G. Fontana, Corrosion Engineering, McGraw-Hill, New York, NY, 1986.

20. E. Aghion, B. Bronfin, in: G.W. Lorimer (Ed.), Proceedings of the Third International Magnesium Conference, Manchester, 1996, pp313-325.

21. M.S. Dargusch, G.L. Dunlop, K. Pettersen, in: Magnesium Alloys and Their Applications, Werkstoff-Informations Gmbh, Wolfsburg, Germany, 1998, pp277-282.

22. R. Ambat, N.N. Aung, W. Zhou, Corr. Sci. **42** (2000) 1433-1455.

23. S.K. Das, L.A. Davies, Mater. Sci. Eng. A 98 (1988) 1-12.

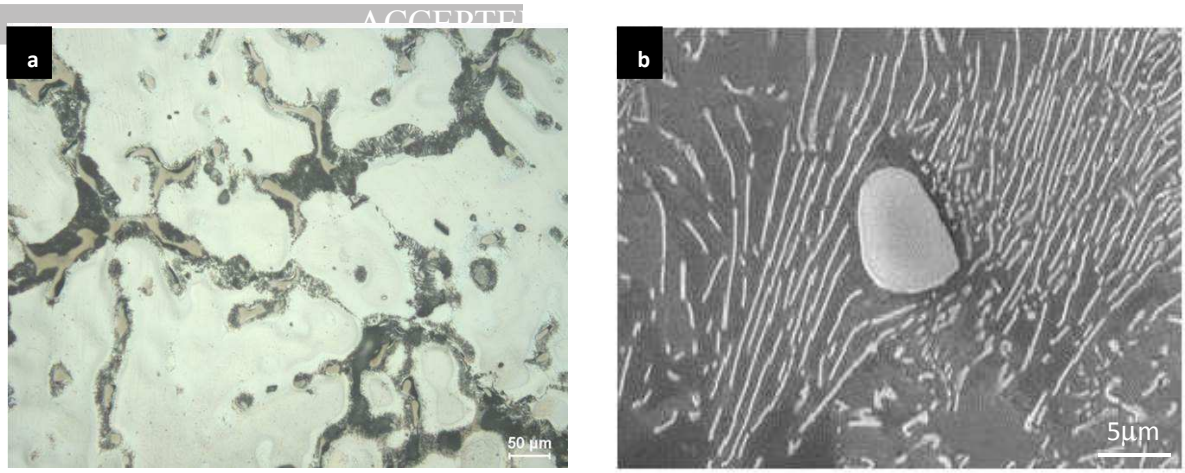

Fig. 1 Microstructure of the as-cast condition: (a) optical micrograph; (b) SEM micrograph.

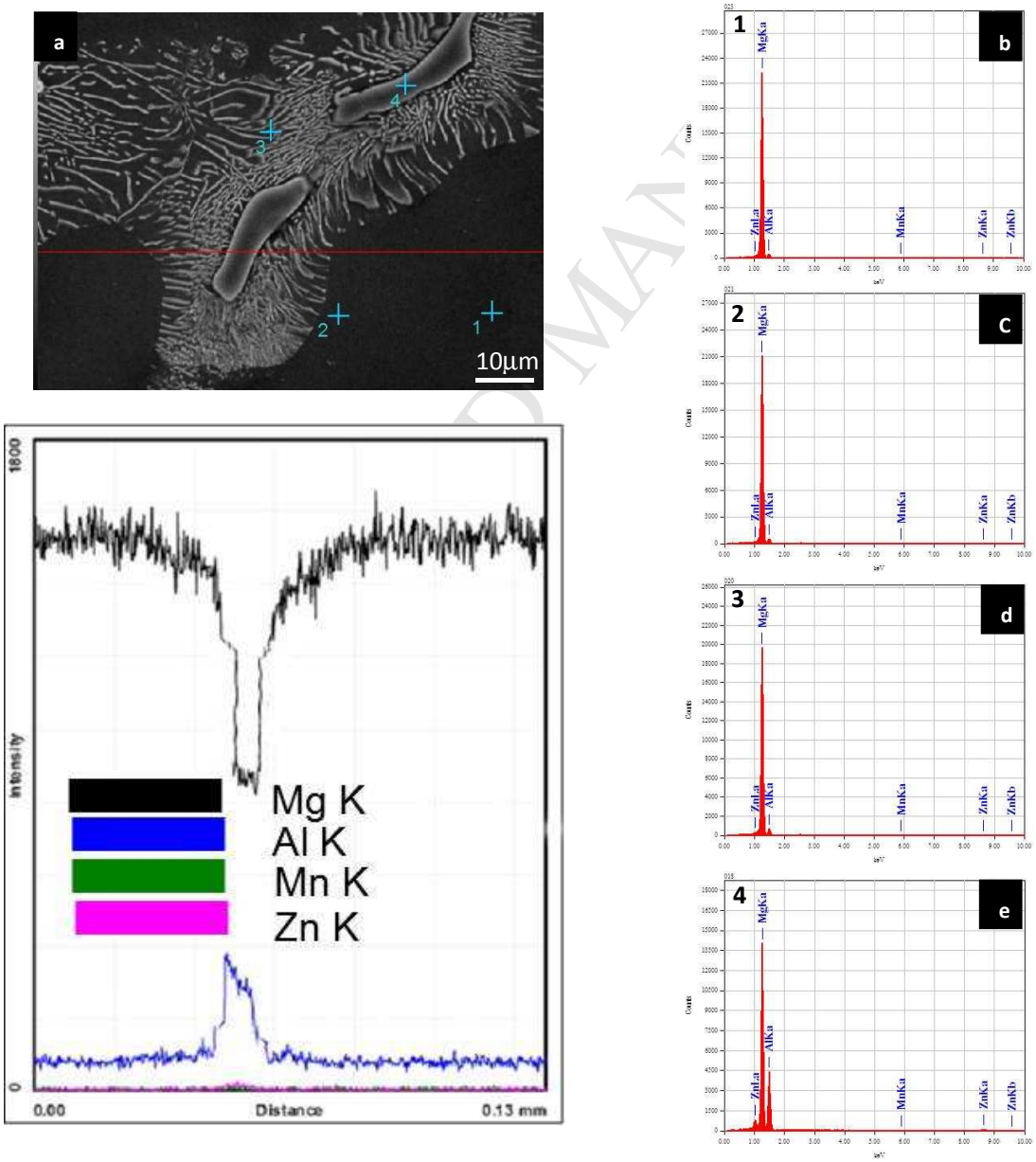

Fig.2 EDS spectra for the as-cast microstructure, presenting the varying composition distribution in different micro-constituents.

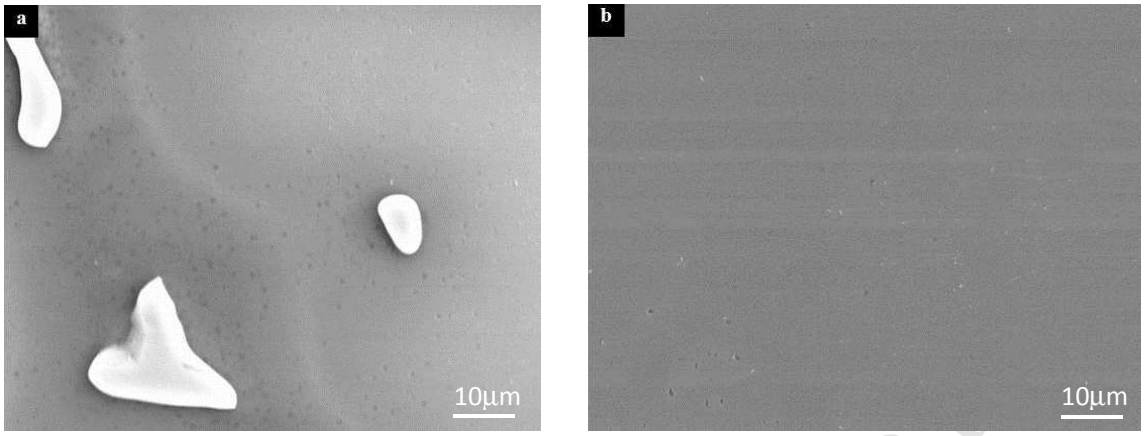

Fig. 3 Microstructures of the comparison 3-S and 4-S conditions as illustrated by SEM micrographs: (a) the 3-S condition; (b) the 4-S condition.

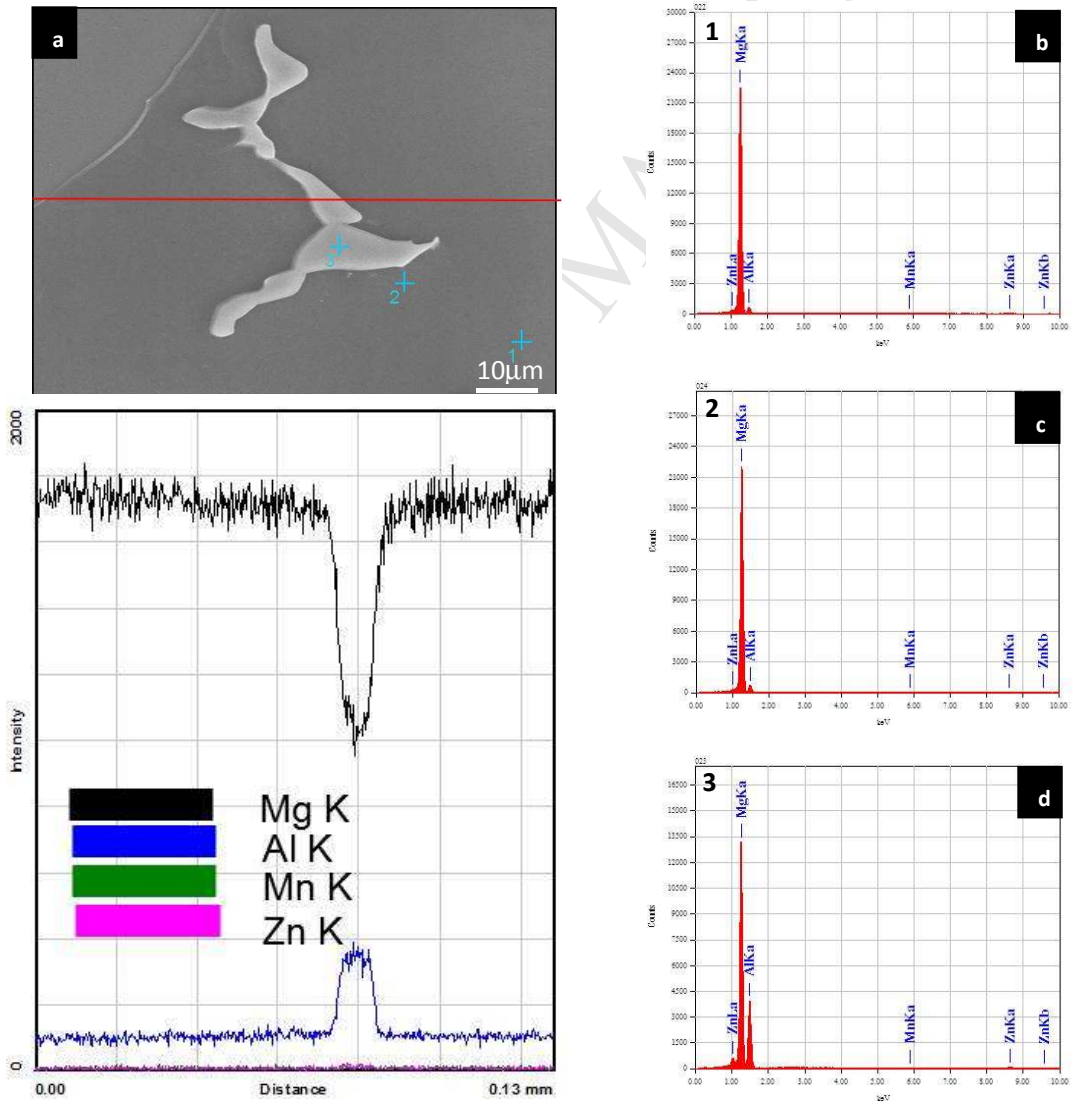

Fig. 4 EDS spectra for 3-S condition showing the varying composition distribution in different micro-constituents.

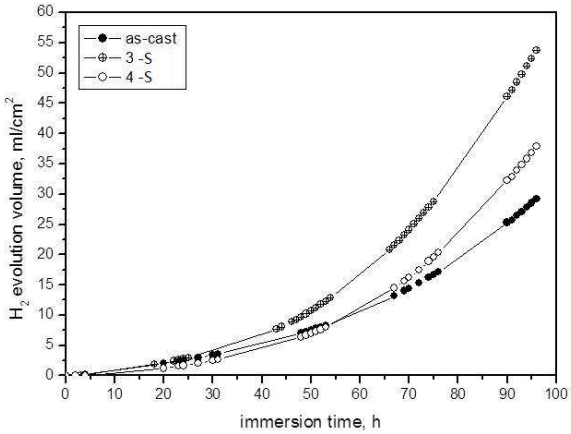

Fig. 5 Plots of H_2 evolution volume versus immersion time.

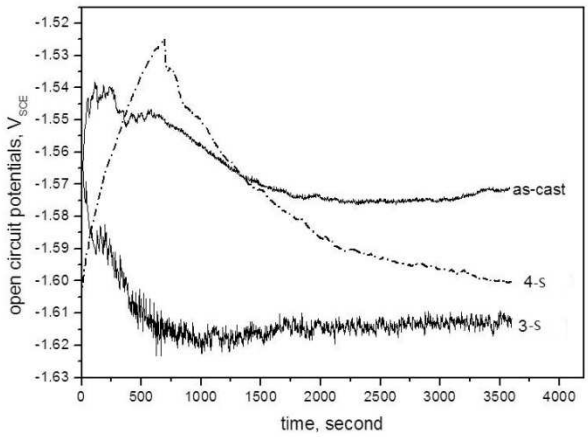

Fig. 6 Variation with time of open circuit potentials.

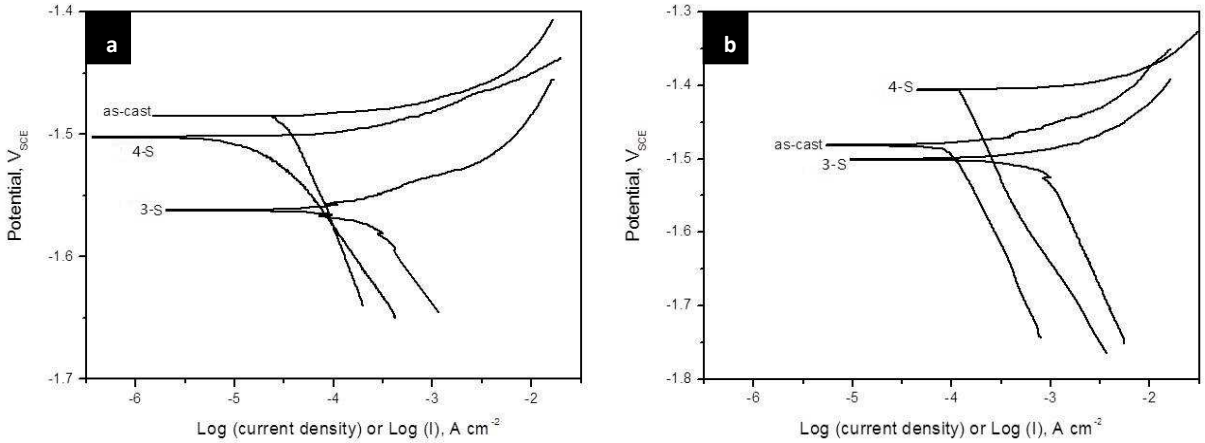

Fig. 7 Polarization curves for (a) immediate immersion and (b) 40 h immersion.

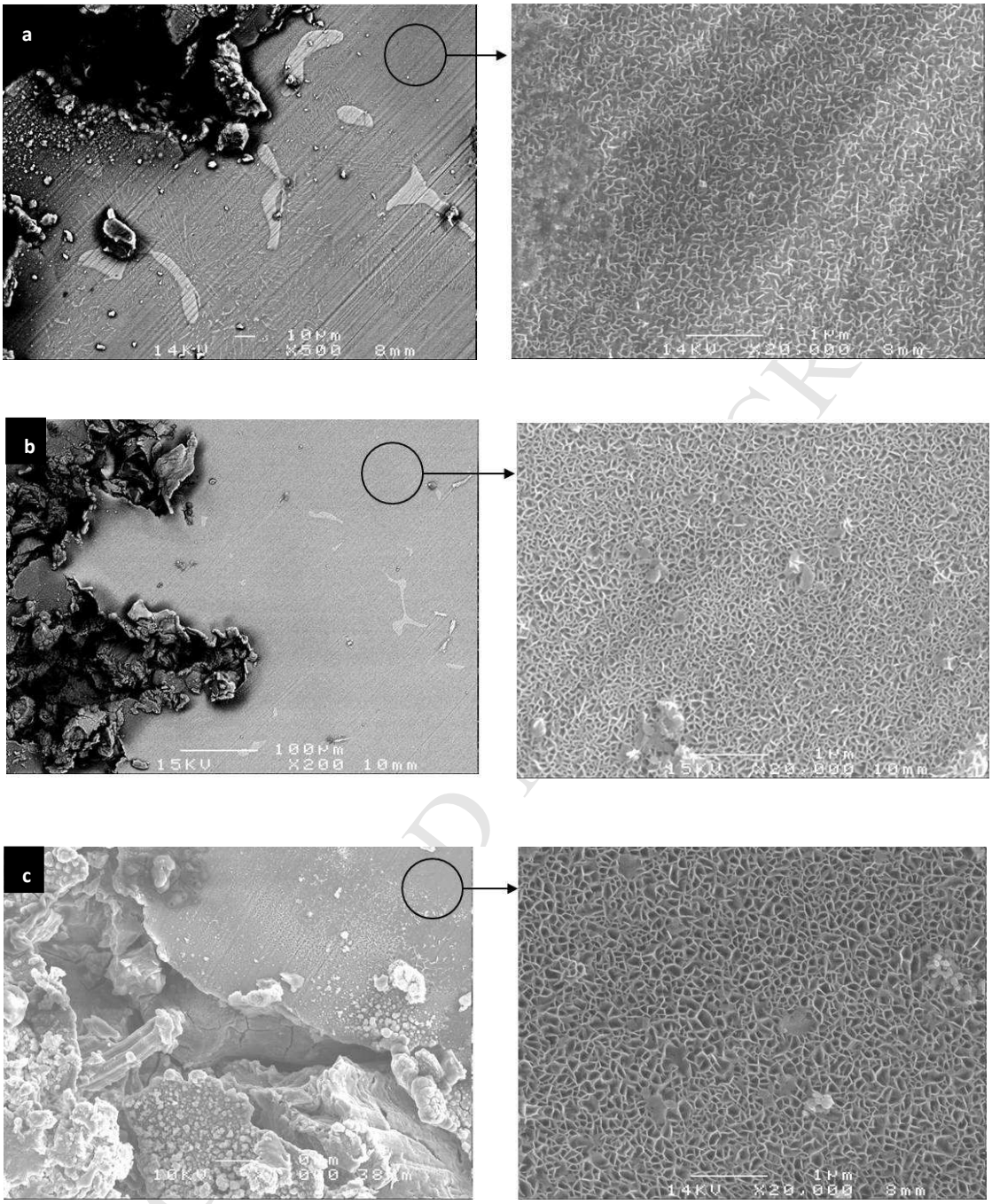

Fig. 8 SEM corroded surface using carbon coated specimen, attacked surface showing exfoliation, spalling and crevice while un-attacked surface coved by a passive film similar to honeycomb in high magnification: (a) as-cast condition, (b) 3-S condition, (c) 4-S condition.

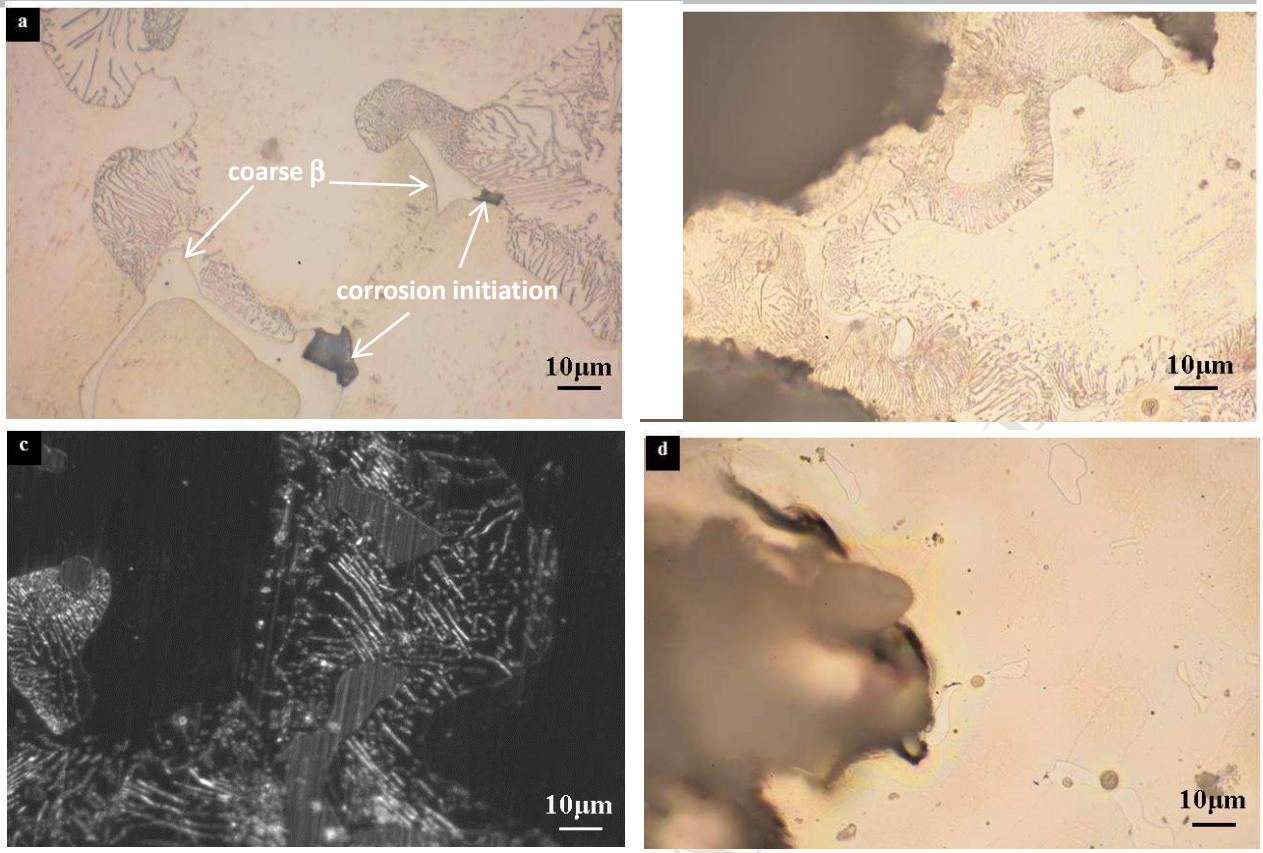

Fig. 9 Micro-corrosion morphology observed by optical microscopy.

(a) 1 h immersion for the as-cast condition; (b) 18 h immersion for the as-cast condition; (c) 36 h immersion for the as-cast condition; (d) 18 h immersion for the 3-S condition.

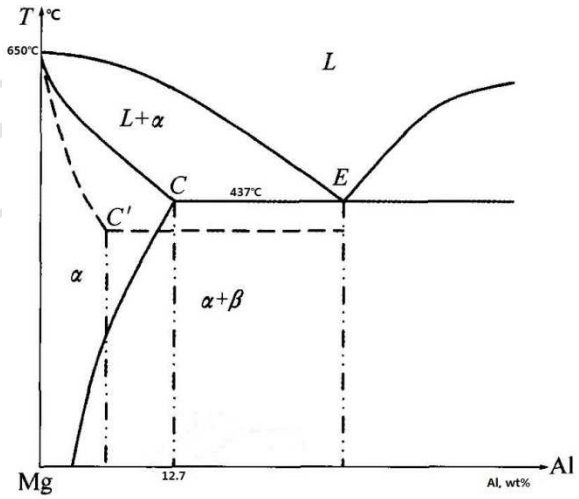

Fig. 10 Mg-Al binary equilibrium phase diagram.

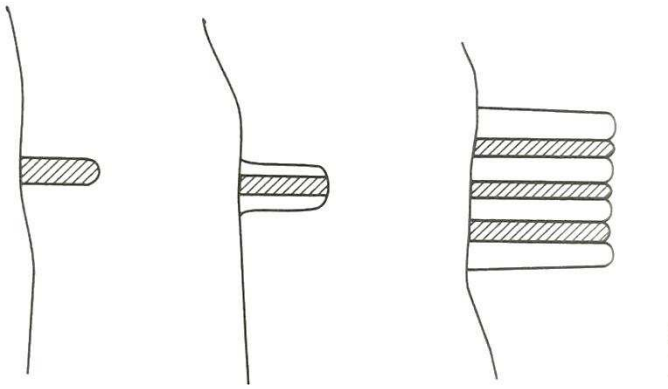

Fig. 11 Schematic illustration of growth process of alternately lamellar arranged fine α plate and fine β plate in as-cast AZ91.

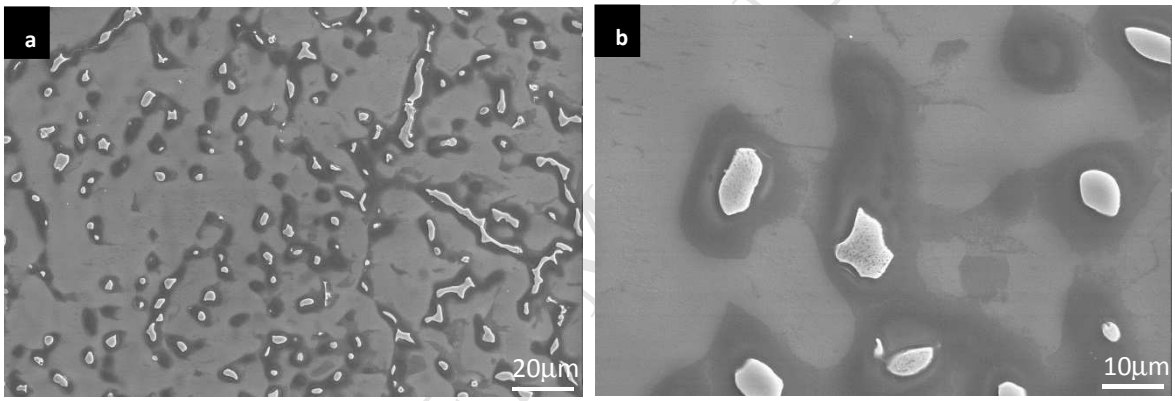

Fig. 12 SEM microstructures for the die-cast condition at varying magnifications.

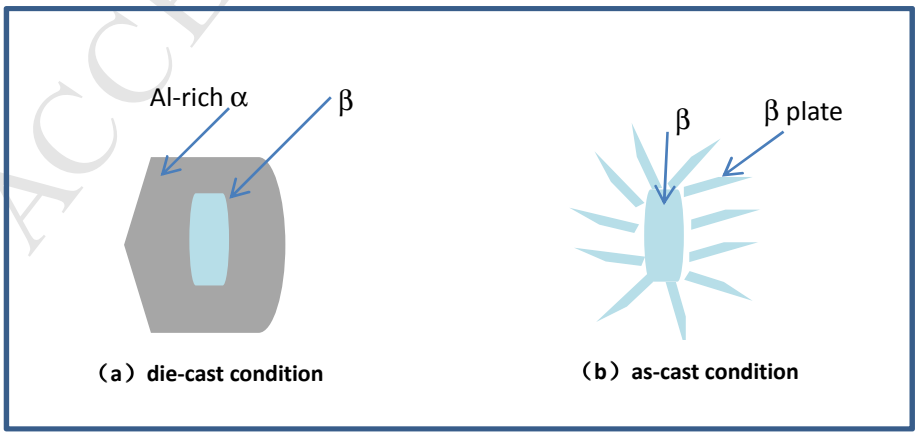

Fig.13 A schematic of the relative sizes of Al-rich α and β for die-cast AZ91 and (α+β) lamellae and β for as-cast AZ91.

- α-Mg grains and coarse β particles derived from the divorced eutectic reaction.
- (α+β) lamellae precipitated from the original eutectic Al-rich-α area.
- The original eutectic Al-rich-α phase was deleterious to corrosion resistance.
- The (α+β) lamellae was beneficial to corrosion resistance.